EPR and luminescence studies of LaF$_3$ and CeF$_3$ under X-ray and laser irradiation

E.D. Thoma[a,*], H. Shields[a], Y. Zhang[a], B.C. McCollum[b], R.T. Williams[a]

[a]*Department of Physics, Olin Physical Laboratory, Wake Forest University, Box 7507, Reynolda Station, Winston Salem, NC 27109, USA*
[b]*Optovac, 24 East Brook Field Rd., North Brookfield, MA 01535, USA*

Abstract

After X-ray irradiation below 70 K, LaF$_3$ exhibits a 3-line EPR resonance consistent with self-trapped holes (V$_k$ centers) on the fluorine sublattice. Specifically, we conclude that the V$_k$ centers are formed on pairs of fluorine ions making $15°$ angles to the c-axis. At temperatures below 200 K, the spectrum of X-ray excited luminescence is dominated by 5d–4f transitions of Ce^{3+} impurity present at 4 ppm. Near room temperature, the transfer to the Ce^{3+} ceases within detectability, revealing a weak band suggested in other work to be self-trapped exciton luminescence. Above 400 K, the 5d–4f transitions of Ce^{3+} again dominate the spectrum, implying resumption of efficient energy transfer from the uniformly distributed X-ray excitations in the LaF$_3$ crystal to the dilute impurity. In CeF$_3$, a 7-line hyperfine EPR pattern at $g = 2$, with isotropic angular dependence, is shown to be composed of independent 3-line and 4-line patterns possessing different thermal and microwave power saturation properties. Such patterns arise from a single electron (or hole) interacting with 2 and 3 equivalent spin-$\frac{1}{2}$ nuclei, respectively.

Keywords: CeF$_3$; LaF$_3$; V$_K$ center; Self-trapped exciton; X-ray; EPR

1. Introduction

Alkali metal fluorides, M$^+$F$^-$, and alkaline earth metal difluorides, M^{2+}F$_2^-$, are well-known paradigms of the simplest ionic crystals, in which both constituent ions have the closed-shell electronic structure of rare gas atoms. In spite of this simplicity of the ground-state structure, and in part because of it [1], the excited states of these crystals are unstable against a lattice distortion which spontaneously localizes or "self-traps" the excitation.

Self-trapped excitons and holes have been extensively studied in alkali and alkaline-earth halides, and have a strong influence on both energy transport and radiation damage [2]. In the series M$^+$F$^-$, M^{2+}F$_2^-$, ..., the next compound family M^{3+}F$_3^-$ includes the rare-earth trifluorides. The simplest of these is LaF$_3$, in which the ions La^{3+} and F$^-$ have the closed-shell rare gas electronic configurations of Xe and Ne, respectively. The valence band is composed mainly of fluorine 2p states [3], just as in the monovalent and divalent metal fluorides cited, and the band gap of LaF$_3$ is about 10.3 eV [4], comparable to the alkali and alkaline

*Corresponding author.

earth fluorides. The question naturally arises as to whether the excited states of LaF_3 exhibit lattice instabilities such as are found in crystals of the LiF and CaF_2 families, with consequent ramifications for energy transport and radiation damage.

Cerium-doped LaF_3 has importance as a new scintillator [5], and is also useful in studies of energy transport in the rare-earth triflouride lattice. Both LaF_3 and CeF_3 exhibit substantial ionic conductivity well below their melting points associated with large anion vacancy concentrations [6,7]. The easy formation of anion vacancies and a high equilibrium vacancy concentration are of interest in optical studies of the defect properties of LaF_3.

Cerium also forms a trifluoride crystal, CeF_3, but trivalent cerium has a single 4f electron lying above the fluorine valence band [3,8]. Transitions between the 5d and 4f levels of cerium in CeF_3 have large oscillator strengths and relatively short lifetimes of 30 ns or less [9]. The short fluorescence lifetime, strong luminescence, high density, and radiation hardness of CeF_3 make it technically one of the best new scintillators for electromagnetic calorimeters on high-luminosity colliding beam experiments in particle physics [10]. Some of the same criteria put it among the attractive new scintillators for medical applications as well [11,12]. Luminescence quenching and energy transfer, particularly as they relate to the somewhat disappointing quantum efficiency of pure CeF_3, have been topics of recent investigations [13–16]. Understanding both the defect properties and energy transport in pure MF_3 crystals and their mixtures is important for all of the applications named above, and certainly for attempting to assimilate a picture of self-trapping tendencies in the series of MF, MF_2, and MF_3.

In the present paper, we present electron paramagnetic resonance (EPR) evidence for V_k centers (self-trapped holes) in LaF_3, following our unpublished preliminary report [17]. Interestingly, V_k centers were not found in CeF_3. A reason for this difference will be discussed. Radzhabov and Nepomnyashiki [18] have attributed an ultraviolet optical absorption band to V_k centers in LaF_3 and find that it is missing in CeF_3. We have studied energy transport to very dilute (4 ppm) Ce impurity in LaF_3 as a function of temperature from 20 to 750 K. At low temperature and at high temperature, the energy transport from LaF_3 host to dilute Ce^{3+} impurity is very efficient, but in the mid-range near room temperature it is very inefficient. At room temperature, we observe a broad, relatively weak luminescence band similar to that reported by Moses et al. and suggested by them to be due to self-trapped excitons [12].

Our EPR data on pure CeF_3 show that the 7-line isotropic resonance previously suggested to be due to F centers or related defects [19] is composed of independent 3-line and 4-line patterns having the same splitting. These are consistent with an unpaired spin interacting with two equivalent spin-$\frac{1}{2}$ nuclei and with three equivalent spin-$\frac{1}{2}$ nuclei, respectively. Assignment to a specific defect has not been possible yet.

2. Experiment

LaF_3 and CeF_3 samples were grown and polished at Optovac. The purest LaF_3 was from a boule grown in 1994 from LaF_3 prepared from 99.999% pure oxide (Rhone-Poulenc, Phoenix, AZ). The material was treated at Optovac prior to crystal growth in order to reduce the oxygen content. The CeF_3 crystal was grown in 1993 at Optovac for the Crystal Clear Collaboration [10]. Both LaF_3 and CeF_3 crystals were grown by the Bridgman–Stockbarger process in which the material is melted in a graphite crucible within an evacuated furnace. Fluorides of good optical quality require a growth enviroment of very low moisture or oxygen which is in part accomplished under diffusion pump vacuum conditions. The evacuable growth chamber consists of a steel bell jar and base plate fitted with sealed throughputs for graphite electrodes, a graphite heater assembly, and a movable support system for the crucible. During a typical growth, the crucible is positioned so that the material for growth is melted almost to the bottom. Then the crystal is formed by freezing from the bottom up by slowly lowering the crucible out of the hot zone of the furnace. Crystals grown for this study are about 1 cm in diameter, but CeF_3 and LaF_3 can be routinely grown in diameters of 3 cm or larger and lengths up to 15 cm. Crystals were

oriented by X-ray diffraction before cutting and polishing.

The ultraviolet transmission spectra of the 1994 LaF_3 crystals exhibit little structure in the fundamental absorption edge region and a transparency range ($\alpha < 3\,cm^{-1}$) up to 10 eV, indicating good overall purity. By comparison of the optical absorption in the Ce 4f–5d transitions with characterized samples, it was found that the 1994 pure LaF_3 has approximately 4 ppm Ce^{3+} as a trace impurity. Optovac LaF_3 and $La_{1-x}Ce_x F_3$ crystals grown in 1975 and used for the measurements reported by Moses et al. [12] were loaned to us by those authors for comparison measurements. In these crystals, the cerium fraction was $x = 10^{-2}$, 10^{-4}, and $< 5 \times 10^{-5}$, the latter being nominally pure LaF_3.

For low-temperature measurements, samples were mounted in thermal contact with the cold finger of a closed-cycle helium refrigerator, using silicone grease, Cu-based "crycon" grease, or indium foil. A fused silica vacuum shroud enclosed the sample for insertion in the EPR cavity, and was used for some of the luminescence experiments. Neither the greases nor the fused silica produced significant luminescence relative to the sample spectra under X-ray excitation. The greases showed no X-ray induced EPR resonances in the range of interest for this work, but the fused silica shroud accumulated defects with a resonance near $g = 2$ after repeated irradiations. However, the fused silica shroud remained at room temperature as the sample temperature was changed. It was possible to distinguish the single-line fused silica resonace from the signals of interest through their temperature dependence and details of the spectrum.

The tungsten-target X-ray source was operated at 40 keV and 10 mA, with the sample placed 1 in from the tube window in irradiations for EPR studies, and about 3 in from the window for luminescence measurements. In all EPR experiments the X-ray beam passed through the fused silica vacuum shroud (0.5 mm wall thickness) before reaching the sample. For X-ray excited luminescence experiments, the crystal was irradiated through either the fused silica vacuum shroud or through a Be window. No differences in spectra were noted. Preparation for EPR experimentation involved X-

ray irradiation for 2–3 h. EPR spectra were recorded using a Varian E-line spectrometer. DPPH was used as a marker and a strong pitch sample was used for spin concentration comparisons. Samples were irradiated at 25 K and maintained at that temperature in the dark during insertion of the cold finger into the EPR cavity. The refrigerated sample fixture allowed incremental rotation of the crystal axis orientation with respect to the magnetic field direction, over a range of $\pm 90^\circ$. The sample could be irradiated by light from a laser or a lamp during EPR measurements. The fourth harmonic of light from a Q-switched Nd:YAG laser (3 ns, 266 nm) was used in this way to form defects in CeF_3.

3. Results and Discussion

3.1. EPR investigation of LaF_3

EPR spectra of the 1994 LaF_3 crystal are presented before and after irradiation in Fig. 1. The spectra were recorded for a microwave frequency of 9.27 GHz and for the data of Fig. 1 the magnetic field was aligned along the crystal c-axis. Fig. 1(a) is the spectrum observed at a temperature of 25 K before X-irradiation. The preirradiation spectrum shows an unknown impurity with $g = 2$. The concentration of the impurity is estimated to be about 40 ppm from a comparison of the impurity signal intensity with that from a standard pitch sample. The peaks in Fig. 1(a) are narrow when the magnetic field is aligned along the c-axis, but split into multiple components when the magnetic field is rotated as little as $\pm 5^\circ$ away from the c-axis. The spectrum shown in Fig. 1(b) was observed under the same conditions as Fig. 1(a), except that the LaF_3 had been irradiated at 25 K. The impurity spectrum is not noticeably affected by the x-irradiation, but the irradiation produced three new peaks at $g \approx 2.0$, having equal splittings of 870 G between adjacent lines. The two outside peaks and about $\frac{2}{3}$ of the central peak anneal between 60 and 70 K [20], as illustrated in Fig. 2. When the residual intensity of the central peak is subtracted from its initial intensity, the intensity ratios of the triplet peaks which anneal are close to 1:2:1. The residual signal at the position of the central peak may be
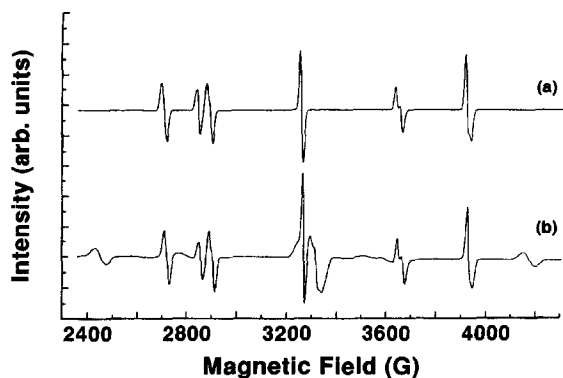
Fig. 1. EPR spectra of LaF$_3$ before (a) and after (b) X-irradiation at 25 K. The observation temperature was also 25 K. The magnetic field was parallel to the c-axis of the crystal.
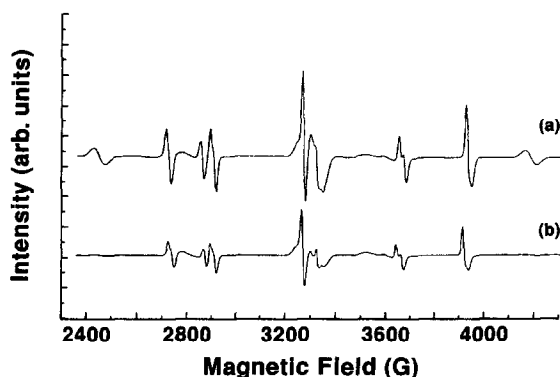

Fig. 2. EPR spectra of LaF$_3$ after X-irradiation at 25 K. Trace (a) was taken at a fixed temperature of 25 K. Trace (b) was taken while the temperature of the crystal was increasing at a rate of 5 K/min and spans a range from 73 to 78 K. The magnetic field was parallel to the c-axis. The signal gain was the same for both traces.

from defects produced by irradiation of the quartz shroud or other radiation induced defects in LaF$_3$.

The radiation-induced triplet pattern seen in Fig. 1(b) is attributed to a hole trapped on two adjacent fluorine ions, i.e. a V$_k$ center. In the V$_k$ center, the unpaired electron interacts equally with the two halogen nuclear spins. Since the fluorine nuclear spin is $\frac{1}{2}$, this hyperfine interaction gives a triplet EPR spectrum near $g = 2.0$ with intensity ratios of $1:2:1$ as observed. The hyperfine interaction for the V$_k$ center is anisotropic with principal

values for the coupling parallel and perpendicular to the F$_2^-$ molecular axis. Because of the impurity signal, we were unable to follow the angular dependence through a range of angles sufficient for determining the principle values of the coupling. The principal values in the perpendicular and parallel directions are typically about 900 G and 60 G, respectively, for the V$_k$ centers in the metal fluoride crystals [21–23]. The observed value of 870 G in irradiated LaF$_3$ when the magnetic field is along the c-axis suggests that the molecular axis of the V$_k$ center is very close to the c-axis of the crystal.

The LaF$_3$ crystal structure, D$_{3d}^4$ (P-3c1) [24], is shown in perspective view in Fig. 3(a) [25]. Fig. 3(b) shows the projection of one cell onto the a, b plane. In the perspective view of Fig. 3(a), it can be seen that the tysonite structure is composed of alternating pure fluorine puckered planes and mixed planes containing lanthanum and fluorine in approximate hexagonal arrays. The fluorines in the puckered layers are denoted F1, while F2 and F3 refer to slightly different sites in the hexagonal nets. There are six formula units (24 atoms) per unit cell, with 18 fluorines being divisible into 3 distinct subgroups according to symmetry. The F1 sublattice accounts for 12 of the fluorine sites while F2 and F3 sublattices possess 4 and 2 atoms per cell, respectively. There is only a minor crystallographic distinction between the F2 and F3 sublattices. An analysis of the crystal structure gives the possible fluorine pair atomic distances and the angles between the molecular axes of the pairs and the c-axis. These distances and angles are listed in Table 1. We suppose that the most probable sites for the formation of the V$_k$ center may be the pairs with the shortest atomic separations. The pairs with the shortest atomic separations, 2.568 Å, are composed of F1 fluorines which lie along lines making angles of 15° with respect to the c-axis, see Table 1. The 15° angle agrees with the conclusion from the EPR data that the molecular axes of the observed V$_k$ centers are oriented near the c-axis. In fact, the 15° pair is the only type of close fluorine pair making a small, nonzero angle with the c-axis. Two other sets of pairs are oriented exactly along the c-axis. Not only would these sites fail to give the observed splittings of the hyperfine lines as the crystal is rotated, but their separation, 3.767 Å, is larger than
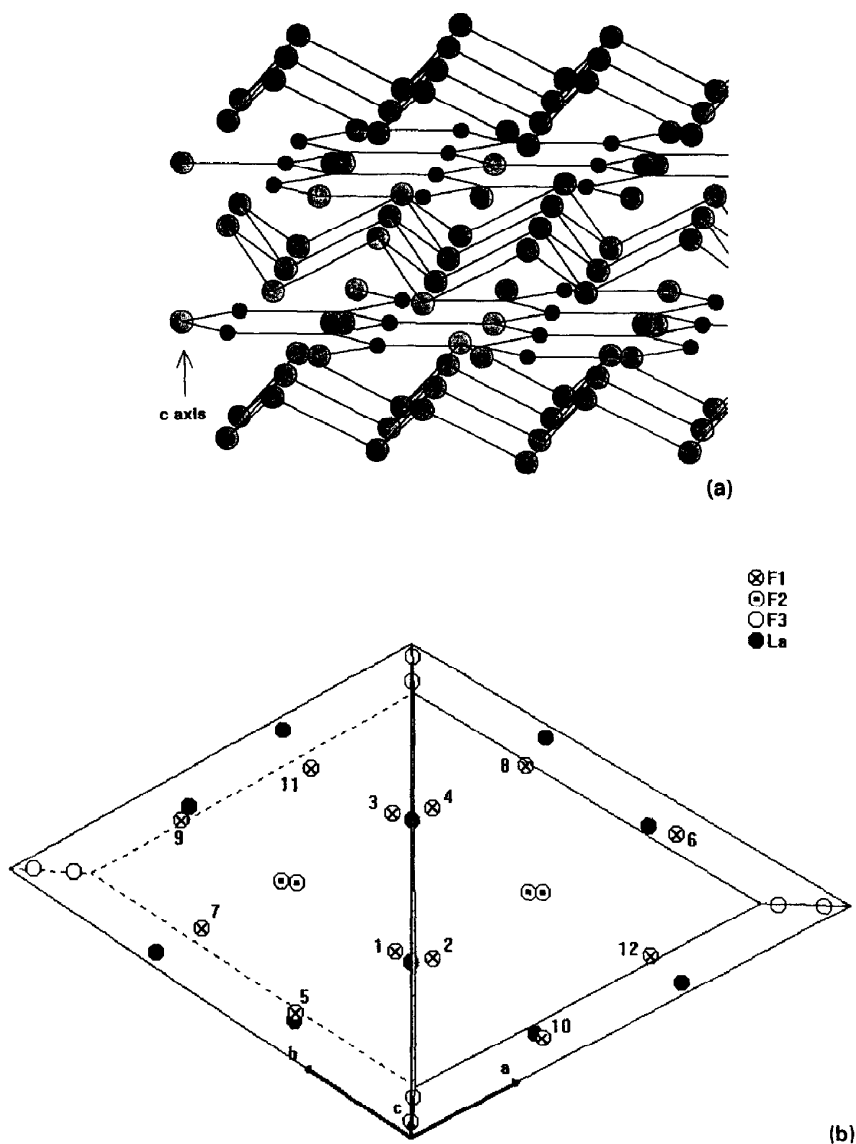
Fig. 3. (a) Perspective drawing of the tysonite structure of LaF$_3$ (courtesy of Alov [25]). (b) LaF$_3$ unit cell with fluorine positions considered to participate in the V$_k$ centers shown in bold and numbered (1-2, 3-4, 5-6, 7-8, 9-10, and 11-12 are pairs). The a,b plane is parallel to the plane of the page. (c) A simplified model of the three equivalent F1-F1 V$_k$-center orientations. The three pairs share a common atom for simplicity. The pairs exhibit C$_{3v}$ site symmetry.

2.568 Å. All other possible pairs have separations larger than 2.568 Å, and they also have large angles with respect to the c-axis, which would result in hyperfine splittings much smaller than that observed, and a larger angular dependence for small excursions from $c\|H$.

The identification of the fluorine atoms forming the F1 pairs oriented with their molecular axis 15° from the c-axis are listed in Table 2. Referring to Fig. 3(a), these pairs are composed of one fluorine from each of two puckered F1 layers on opposite sides of the lanthanum hexagonal net layer. The
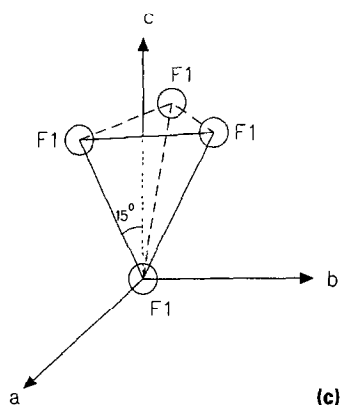
Fig. 3. Continued.

Table 1
Possible fluorine pair atomic distances and angles between the molecular pair and the c-axis.

	Distance (Å)	θ_c(deg)	Number of orientations	Number of pairs
F1–F1 (min)	2.568	15.0	3	6
F1–F1 (4–1)	2.687	63.6	3	6
F1–F1 (10–1)	2.734	64.1	3	6
F2–F2 (min)	3.767	0	1	2
F2–F2	4.254	77.2	1	2
F3–F3 (min)	3.767	0	1	1
F1–F2 (min)	2.701	50.7	6	12
F1–F2	2.868	46.8	6	12
F2–F3 (min)	4.175	83.5	3	12
F1–F3	2.754	63.2	6	12

Table 2
Angles between the crystal axes and the molecular axis of F1–F1 fluorine pairs proposed to form the V_k center. See Fig. 3(c) for a simplified representation of these pairs

	Distance (Å)	θ_c(deg)	θ_a(deg)	θ_b(deg)
1 → 2 3 → 4	2.568	15.0	103.0	77.0
5 → 6 7 → 8	2.568	15.0	90.0	103.0
9 → 10 11 → 12	2.568	15.0	77.0	90.0

value of the coupling constant parallel to the axis of the V_k center is estimated from the relation $A \approx A_\parallel \cos(15°)$, where A is the splitting observed with the field 15° from the c-axis and $A_\parallel$ is the

Table 3
Magnetic coupling constants of V_k centers in various fluoride crystals. Data on LiF, NaF, KF and RbF were taken from Ref. [23] and data on LiYF$_4$ were taken from Ref. [26]

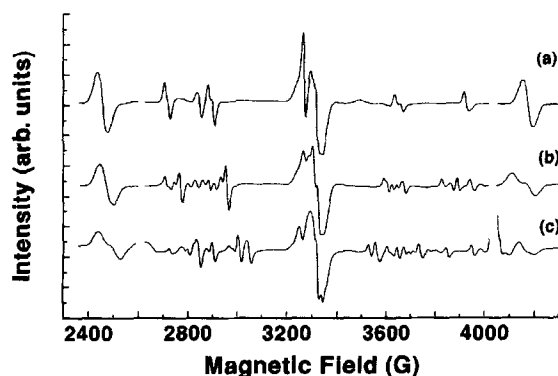| Materials	Coupling (G)
LiF	883.7
NaF	897.1
KF	908.0
RbF	908.4
LiYF$_4$	875.2
LaF$_3$	900

Fig. 4. EPR spectra of LaF$_3$ (4 ppm Ce) after X-irradiation at 25 K with the magnetic field at three different angles to the c-axis. Trace (a) was taken with H along the c-axis. Trace (b) displays the signal after a 10° rotation of the crystal about an axis perpendicular to the c-axis (H at 10° to the c-axis). Trace (c) shows a 20° rotation about the same axis. The receiver gain during the scan of the outer V_k center peaks was increased by a factor of 4 relative to the center portion of the scan.

splitting along the V_k axis. A calculated value of 900 G compares favorably with values from other materials listed in Table 3 [21–23, 26].

The orientation of the V_k centers is shown in Fig. 3(c), where the coordinates of the fluorine pairs have been translated to the same origin. When the magnetic field is rotated away from the c-axis, splitting of the spectra as shown in Fig. 4 is expected. The field moves closer to alignment with some pairs and away from others. The splitting cannot be followed beyond a rotation of 20° because of

interference from the impurity spectra. Different splitting of the high and low field peaks is attributed to magnetically inequivalent V_k centers (centers with different orientations with respect to the magnetic field) which have different g-values and hyperfine splittings when the magnetic field makes different angles with the molecular axis.

The widths of the outside peaks in the V_k spectra of LaF_3 are around 80 G (c-axis$\|H$). This is larger than for V_k centers in the alkali fluorides which range from 2.6 G in KF to 12.9 G in LiF. However, when the large dispersion in line widths of V_k centers in the structurally similar alkali fluorides is considered along with the more complicated nature of the tysonite lattice, the observed line widths in LaF_3 seem plausible.

3.2. EPR Investigations of CeF_3

Despite points of similarity between CeF_3 and LaF_3 noted earlier, EPR investigations on X-ray and laser-irradiated (1993 Optovac crystal) CeF_3 yield quite different results. After exposure to X-irradiation at 30 K there is no V_k center spectrum in CeF_3, but there is a seven-line spectrum similar to the one observed by Halliburton et al. [19] in Ba-doped CeF_3, which they attributed to F centers or related defects. An F center, which is an electron trapped at a halogen vacancy, is reasonably well understood in simple crystals such as the alkali halides, but may exhibit more complicated behavior in crystals with a large unit cell and noncubic structure such as CeF_3. The suggested association of the 7-component spectrum with an F center may be based mainly on the location of the spectrum at $g = 2$ and on the isotropic angular dependence of the resonance. The g-value, the width of the peaks, and their magnetic splitting do not vary significantly when the magnetic field is rotated away from the c-axis.

Fig. 5(a) displays EPR spectra of the CeF_3 crystal at 38 K before irradiation, and Fig. 5(b) shows the spectrum under the same conditions after 3 h of X-irradiation. The spectra displayed in Fig. 5 span a magnetic field range of 2000 G centered near 3319 G with the magnetic field parallel to the c-axis. Spectrum 5(b) was taken at slightly lower gain. The observed EPR lines in Fig. 5(a) are
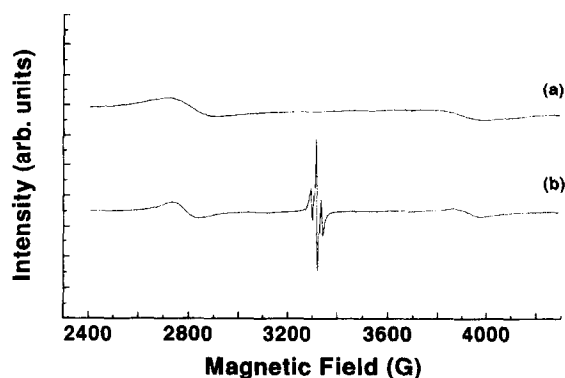

Fig. 5. EPR spectra of CeF_3 before (a) and after (b) X-irradiation at 38 K. The observation temperature was also 38 K. The magnetic field was parallel to the c-axis.
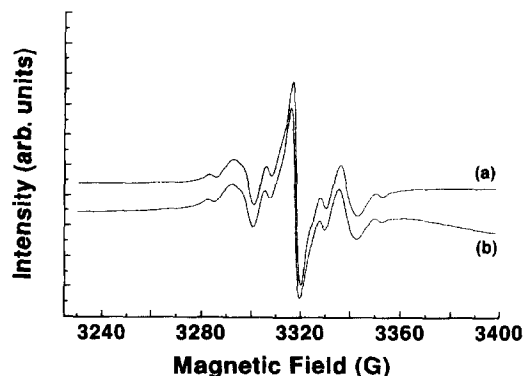

Fig. 6. EPR spectra of CeF_3 after X-irradiation at 38 K with the magnetic field at two different angles to the c-axis. Trace (a) was taken with H along the c-axis. Trace (b) shows the signal after a 45° rotation of H about an axis perpendicular to the c-axis.

believed to be from an impurity, but it has not yet been identified. The X-ray induced lines in Fig. 5(b) centered at $g = 2$ have a total splitting of about 75 G, and they appear in a portion of the spectrum where there are no resonances from the impurity at temperatures below 200 K. The spectra in Fig. 6 show the same defect signal as in Fig. 5 with a 200 G sweep. A 7 line hyperfine pattern is discernible. Spectrum 6(a) was taken with the magnetic field along the c-axis. Spectrum 6(b) was obtained after a 45° rotation away from the c-axis and is identical to spectrum 6(a) except for a slight shift in the g-value.
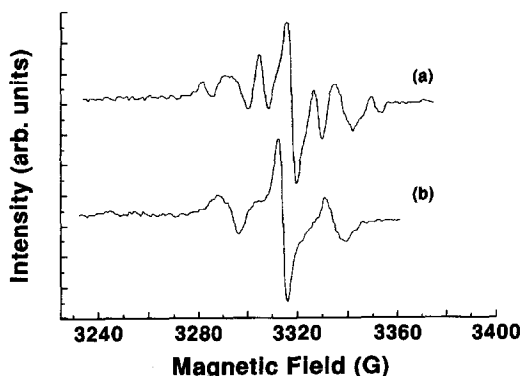
Fig. 7. EPR spectra of CeF_3 after irradiation at 40 K with 266 nm, 3 ns laser pulses at energy density 0.320 mJ/cm². Trace (a) was taken at an observation temperature of 96 K. Trace (b) was taken at 135 K. Spectrum (b) has been offset by -5 G for ease of viewing.

Annealing of the defects responsible for the resonance was investigated while warming the sample after 266 nm irradiation at 40 K as shown in Fig. 7. Spectra 7(a) and (b), taken at 95 and 135 K, respectively, demonstrate that not all of the 7 hyperfine lines arise from the same center. Spectra 7(b) has been offset by -5 G for clear viewing. The relative intensities of the components in the 7 component spectrum observed at 40 K began to change as the temperature was raised above 100 K. The intensity of a quartet begins to decrease rapidly at 120 K relative to a triplet. Whereas the quartet disappears at about 140 K, the intensity of the remaining triplet at 140 K is still near its maximum. Because there is no significant change in the triplet intensity from 40 to 130 K, it appears that the center responsible for the quartet spectrum is not transforming to the triplet center; presumably, it changes to a nonparamagnetic species. The intensity ratios $(1:3:3:1)$ and equal splittings of the quartet indicate that this is due to the hyperfine interaction of an unpaired electron spin with three nuclear spins of $\frac{1}{2}$. Likewise the triplet spectrum approximates the intensity ratio $(1:2:1)$ expected from an equal hyperfine interaction with two nuclear spins of $\frac{1}{2}$. The hyperfine splitting between the peaks in the quartet and the triplet is 22 G. In each case the spectrum could result from an unpaired spin interacting with fluorine nuclei. In the triplet the outside peaks are partially split indicating that the interac-

tion is not quite equal. Similar annealing results were obtained with defects created by X-irradiation. Since cerium has no nuclear spin, the triplet and quartet patterns would have to result, in an F center model, from interaction of the trapped electron with fluorines in the second shell of the neighbor ions, beyond the cerium nearest neighbors. Futhermore, the neighbor fluorines would have to be arranged in 2 and 3 equivalent sites relative to the fluorine vacancy at one of the 3 sites F1 ... F3. More work, both theoretical and experimental, is required to understand this center. An impurity center with hyperfine interaction from hydrogen is another possibility. EPR from atomic hydrogen was observed after X-irradiation at 30 K.

The same paramagnetic species were also observed during and after irradiation with 266 nm laser light at low temperature. The laser pulse energy density was about 0.320 mJ/cm² in 3 ns pulses at 10 Hz. The results were similar to those observed after X-irradiation, even though 266 nm (4.66 eV) light is non-ionizing in CeF_3 [3,27]. The growth of the triplet and quartet signals as a function of cumulative 266 nm irradiation dose at low temperature was monitored and found to saturate approximately as the square root of the dose.

The fact that V_k centers were found in LaF_3 but not CeF_3 is understandable in view of the 4f electron remaining in Ce^{3+}. In LaF_3, the fluorine orbitals forming the V_k state in the gap are stable hole traps because there are no higher filled electron orbitals in the perfect LaF_3 electronic structure. In contrast, if the Ce^{3+} 4f electron state lies above the V_k level in CeF_3, there is a ready supply of electrons to annihilate the V_k hole. Electron capture from the 4f state to the V_k center may be rather slow, but probably not on the scale of several minutes required to obtain EPR spectra after X-irradiation.

3.3. Luminescence

The spectroscopic properties of $Ce_xLa_{1-x}F_3$ have been studied extensively in recent years [5,9–13,28–35]. Despite some differences in luminescence spectra and decay times for differing excitation, geometries, and crystal purity, all investigations agree on the presence of two main luminescence bands, the intrinsic and extrinsic
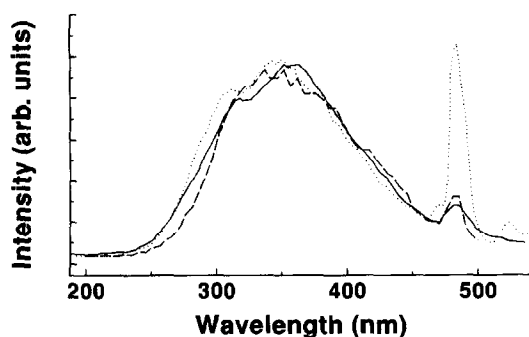
Fig. 8. Room temperature luminescence in nominally pure LaF$_3$ under X-ray and 20 eV excitation: (——) X-ray induced luminescence from 1994 LaF$_3$; (····) X-ray luminescence from 1975 LaF$_3$; (— — —) linear scale replot of 20 eV excited luminescence of 1975 LaF$_3$ taken from Ref. [36].

Fig. 9. X-ray induced luminescence in LaF$_3$ (4 ppm Ce) at various temperatures: 700, 460, 375, 330, 293, 270, 220, 160 and 33 K. The 160 K trace has been divided by 3. The 33 K trace has been divided by 1.5.

emissions. The intrinsic emission comprises the pair of Ce^{3+} 5d–4f spin–orbit-split transitions at 285 and 300 nm. This short wavelength luminescence (swl) exhibits fast (15–30 ns) and very fast (2–10 ns) decay times with very fast rise times. The extrinsic band at 340 nm is ascribed to perturbed-site Ce^{3+} 5d–4f emissions [32]. The perturbed band is also known as the long wavelength luminescence (lwl) band and possesses a slow rise time and >30 ns decay constant. The nature of the perturbing species is unknown.

Moses et al. [12] have observed a broad luminescence band centered near 360 nm in nominally pure LaF$_3$ under 20 eV excitation. They have tentatively ascribed this emission to self-trapped exciton luminescence. We have found the same broad emission band in both 1975 LaF$_3$ and 1994 high purity LaF$_3$ under X-ray excitation. These luminescence spectra are presented in Fig. 8. Luminescence intensities are in arbitrary units. The dashed line spectrum is a replot on a linear scale of luminescence from 1975 LaF$_3$ under 20 eV excitation at room temperature, reported in Refs. [12, 36]. The sharp peak at 480 nm has been attributed to praseodymium impurity luminescence [36]. The dotted line spectrum in Fig. 8 is X-ray excited luminescence from the same crystal at room temperature taken during this study. The wide band (about 100 nm FWHM) is clearly present. The solid line trace is X-ray excited luminescence from the high-purity
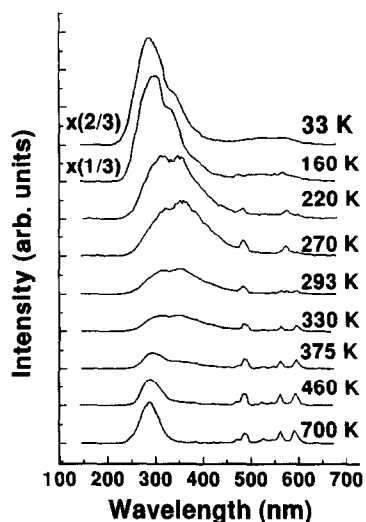
1994 LaF3 sample (Ce $= 4 \times 10^{-6}$). Again the wide band is detected, but there is much less relative contribution from the Pr impurity in the 1994 sample. The X-ray excited spectrum at room temperature in the 1994 LaF$_3$ appears to be composed of at least two bands: one centered near 330 nm and the other at about 370 nm. The wide (possibly multicomponent) room temperature luminescence band in nominally pure LaF$_3$ is therefore consistently produced in crystals of differing origins and excitation energies.

Spectra of X-ray excited luminescence in the temperature range 33–700 K are compared in Fig. 9. The X-ray excited luminescence bands at 33 and 160 K are much brighter than at higher temperatures, and have been multiplied by factors of $\frac{2}{3}$ and $\frac{1}{3}$, respectively, for comparison purposes. The most intense part of the spectrum from 280 to 305 nm is the (unresolved) spin–orbit-split intrinsic 5d–4f transition (swl) on the dilute Ce impurity. As temperature is increased from 160–293 K, the swl light yield decreases dramatically. This band is essentially undetectable around room temperature. As temperature is raised above room temperature ($T > 400$ K), a band reappears near 290 nm which
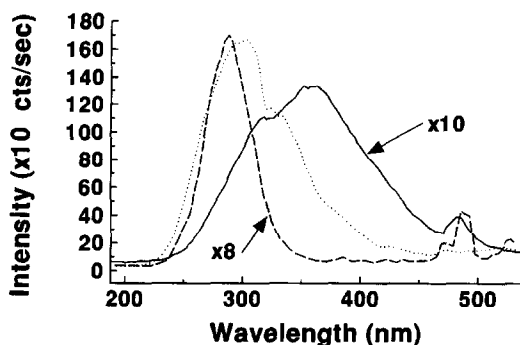
Fig. 10. X-ray excited luminescence from LaF_3 (4 ppm Ce) at three temperatures: (———) 293 K, (·····) 165 K, (– – –) 700 K. The $T = 293$ K and the $T = 700$ K spectra have been multiplied by factors of 10 and 8, respectively.

may also be ascribed to Ce swl. Thus, the quenching at room temperature is not due to non-radiative crossing to the ground state. Rather, it may be due to a thermally activated loss of energy transport from the LaF_3 host to the dilute Ce^{3+} impurity. That is, there is a thermally activated trapping of carriers or excitons, in contrast to the more usual thermal detrapping. The peaks at 560 and 590 nm are probably due to other rare earths present in trace levels.

Fig. 10 compares X-ray excited luminescence spectra from 1994 LaF_3 at $T = 165$ K, $T = 293$ K, and $T = 700$ K. The $T = 293$ K and $T = 700$ K spectra have been multiplied by factors of 10 and 8, respectively. The high temperature ($T > 400$ K) swl band at 290 nm differs form the $T = 165$ K swl emission which is accompanied by a shoulder at 330 nm reminiscent of the (lwl) luminescence described earlier. Careful comparison suggests that this shoulder may also contribute to the $T = 293$ K luminescence. The 1975 $Ce_xLa_{1-x}F_3$ ($x = 1 \times 10^{-4}$ and $x = 5 \times 10^{-5}$) crystals exhibit similar spectral changes with temperature, but there is more low-level luminescence extending to long wavelengths.

Two examples of thermally activated deep trapping known from other systems are self-trapping of charge carriers and excitons in pure crystals [2], and extrinsic self-trapping or bistability of defect states in defective crystals [37]. In alkali halides, it is well known that there are thermal barriers against relaxation of the exciton to the self-trapped

state. For example, in KI there is free exciton transport of energy in band states for temperatures below about 40 K (30 meV barrier) [38]. After self-trapping, the excitons can only transport energy by hopping mobility. It is worth noting the holes and excitons can have quite different barriers to self-trapping, in the same material. Hole self-trapping in ionic crystals is driven by the combined effects of short-range (e.g. molecular bonding, deformation potential) and long-range (dielectric polarization) interactions with the lattice. The exciton, on the other hand, is neutral and therefore not strongly benefitted by long-range polarization [2]. For example, in alkali iodides there is no barrier to self-trapping of holes, whereas exciton self-trapping is impeded by the barrier discussed just above. One of the few cases of an observable barrier to hole self-trapping is found in AgCl, where holes self-trap only after surmounting or tunneling a barrier of 1.7 meV [39]. It has been conjectured that in MgO there may be a barrier height of 40 meV against self-trapping of the exciton [40,41], but this is about the highest self-trapping barrier known or conjectured.

Qualitatively, a self-trapping model can explain the observations of Fig. 9 quite well. We can suppose that at low temperature, excitons and charge carriers are mobile in band states, transporting excitation efficiently from the LaF_3 host to the very dilute (4 ppm) Ce impurity. With sufficient thermal energy to surmount the thermal barrier, the carriers of excitation relax into immobile self-trapped states. Energy transport to the Ce^{3+} impurity stops, and recombination must occur at the self-trapping sites, possibly resulting in the 370 nm broad band found near room temperature. However, it is known that self-trapped carriers and self-trapped excitons move by hopping at sufficiently high temperature. Thus in LaF_3, we might conjecture, the self-trapped excitation becomes mobile again as temperature rises from 300 to 700 K, and efficient transport to the dilute Ce^{3+} impurity resumes. This model fits many aspects of the data, but as noted earlier it requires a large barrier to self-trapping, which preserves band mobility up to ≈ 250 K. While not ruled out on any fundamental ground, this would be the largest such barrier yet encountered in regard to intrinsic self-trapping.

Let us consider another example, that of the shallow-deep instability of traps such as the Si center (DX center) in GaAs [42], or the In and Ga centers in CdF_2 [43]. The phenomenon is described in terms of extrinsic self-trapping [44], in which a weak hydrogenic impurity (potential incapable) of deep trapping, and a marginal electron-phonon interaction (strength incapable) of inducing intrinsic self-trapping, are present in the same crystal. Their joint action is to induce a deep-trap state coexisting with the shallow-trap level, but separated by a thermal barrier. Persistent photoconductivity can be observed in such systems when carriers are photo-excited to the shallow-trap potential curve. They can transport charge until they cross to the curve of the deep level, at which point transport stops. One may then imagine that at substantially higher temperature, even the deep level could be thermally ionized and contribute to excitation transport.

Other models proposed to explain the data of Fig. 9 should contain the essential feature of thermally-activated trapping at intermediate temperature. In the hypothesis presented above, we have not attempted to account for the praseodymium or other RE peaks at the same time, but have concentrated on the unique behavior of the Ce^{3+} impurity luminescence.

3.4. Temperature dependence of luminescence yield

Fig. 11 summarizes the temperature dependence of the luminescence intensity in two emission bands in 1994 LaF_3 and 1993 CeF_3 from room temperature to 33 K. The data were produced by monitoring the light output under X-ray excitation at two wavelengths (290 nm and 340 nm), while the temperature was decreased at a rate of 10 K/min. The direction of temperature change from room temperature to low temperature was chosen to avoid possible contributions from stored energy in the large thermoluminescence peaks which we have observed in the case of LaF_3. Monitoring at 290 nm serves to track the Ce^{3+} 5d–4f (swl) emission while observation at 340 nm portrays changes in the established perturbed site luminescence (lwl) of CeF_3 as well as the 330 nm shoulder and broadband room temperature luminescence in LaF_3. The change in emission at a given wavelength is shown
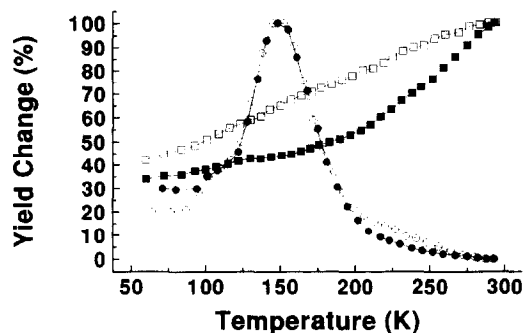

Fig. 11. X-ray excited luminescence output versus temperature in 1994 LaF_3 (4 ppm Ce) and 1993 CeF_3. (—●—) LaF_3 290 nm emission, (—○—) LaF_3 340 nm emission; (—■—) CeF_3 290 nm emission, (—□—) CeF_3 340 nm emission.

as a percentage of the maximum output at that wavelength. The swl in pure CeF_3 is most intense at room temperature and decreases as temperature is lowered. There are several inflections in the yield curve from 110 to 150 K, the same temperature range in which the EPR spectra from CeF_3 annealed (Section 3.2). The 1994 LaF_3 (4 ppm Ce) sample exhibits a much different temperature dependence. The 290 nm emission is completely quenched at room temperature as noted earlier and then dramatically increases as temperature is lowered, peaking at 150 K. The maximum luminescence emission temperature corresponds to the largest of two main thermoluminescence glow curve peaks. The 290 nm X-ray excited luminescence band in LaF_3 increases in intensity in an approximately linear fashion with no discernible inflections from 300 to 700 K.

Acknowledgements

References

[1] R.T. Williams and K.S. Song, J. Phys. Chem. Solids 51 (1990) 679.

[2] K.S. Song and R.T. Williams, Self-Trapped Excitons, Springer Series in Solid-State Sciences 105, (Springer, Berlin, 1993).

[3] K.-H. Park and S.-J. Oh, Phys. Rev. B 48 (1993) 14833.

[4] C.G. Olson, M. Piacentini and D.W. Lynch, Phys. Rev. B 18 (1978) 5740.

[5] W.W Moses and S.E. Derenzo, Nucl. Instr. and Meth. A 299 (1990) 435.

[6] A.F. Aalders, A.F.M. Arts and H.W. de Wijn, Phys. Rev. B 32 (1985) 5412.

[7] F.C. Case and P.P. Mahendroo, J. Phys. Chem. Solids 42 (1981) 385.

[8] L.R. Elias, Wm. S. Heaps and W.M. Yen, Phys. Rev. B 8 (1973) 4989.

[9] A.J. Wojtowicz, M. Balcerzyk, E. Berman and A. Lempicki, Phys. Rev. B 49 (1994) 14880.

[10] P. Lecoq, Mat. Res. Soc. Symp. Proc. 348 (1994) 51.

[11] D.F. Anderson, IEEE Tran. Nucl. Sci. NS-36-1 (1989) 137.

[12] W.W. Moses, S.E. Derenzo, M.J. Weber, A.K. Ray-Chaudhuri and F. Cerrina, J. Lumin. 59 (1994) 89.

[13] A.J. Wojtowicz, A. Lempicki, D. Wisniewski, C. Brecher, R.H. Bartram, C. Woody, P. Levy, S. Stoll, J. Kierstead, C. Pédrini, D. Bouttet and CZ. Koepke, Mat. Res. Soc. Symp. Proc. 348 (1994) 455.

[14] C. Pédrini, D. Bouttet, C. Dujardin, A. Belsky, A. Vasil'ev, 1995 Abstracts of the Int. Conf. on Inorganic Scintillators and their Applications (SCINT-95) (Delft University of Technology, Delft, Netherlands) WE-A-22, p. 13.

[15] A.J. Wojtowicz, 1995 Abstracts of the Int. Conf. on Inorganic Scintillators and their Applications (SCINT-95) (Delft University of Technology, Delft, Netherlands) MO-A-21, p. 3.

[16] M.A. Terekhin, I.A. Kamenskikh, V.N. Makhov, V.A. Kozlov, I.H. Munro, D.A. Shaw, C.M. Gregory and M.A. Hayes, 1995 Abstracts of the Int. Conf. on Inorganic Scintillators and their Applications (SCINT-95) (Delft University of Technology, Delft, Netherlands) MO-A-31, p. 25.

[17] R.T. Williams, E.D. Thoma and H. Shields, 1994 Abstacts of the Int. Workshop on Physical Process in Fast Scintillators (PHYSCI-94) (St. Petersbourg State Technical University, St. Petersbourg) p. Ce6.

[18] E. Radzhabov and A.I. Nepomnyashikh, 1995 Abstracts of the Int. Conf. on Inorganic Scintillators and their Applications (SCINT-95) (Delft University of Technology, Delft, Netherlands) MO-A-41, p. 30.

[19] L.E. Halliburton, G.J. Edwards, Mat. Res. Soc. Symp. Proc. 348 (1994) 423.

[20] In a preliminary oral report on this work at the International Conference on Physics Processes in Scintillators, St. Petersburg, Russia, October 1994, we reported an annealing temperature of 100 K. We regret that this was in error because of too-fast heating rate. The correct annealing temperature of the presummed V_k resonance is 60–70 K as reported in the present work.

[21] T.G. Castner Jr. and W. Känzig, J. Phys. Chem. Solids 3 (1957) 178.

[22] T.O. Woodruff and W. Känzig, Phys. Chem. Solids 5 (1958) 268.

[23] C. Edward Bailey, Phys. Rev. 5A, 136 (1964) 1311.

[24] A. Zalkin and D.H. Templeton, Acta Crystallogr. B 41 (1985) 91.

[25] We thank D.L. Alov for preparing the perspective view.

[26] G.M. Renfro, L.E. Halliburton, W.A. Sibley and R.F. Belt, J. Phys. C13 (1980) 1941.

[27] D.L. Alov and A.V. Bazhenov, 1995 Abstracts of the Int. Conf. on Inorganic Scintillators and their Applications (SCINT-95) (Delft University of Technology, Delft, Netherlands) MO-A-35, p. 29.

[28] D.F. Anderson, Nucl. Instr. and Meth. A 287 (1990) 606.

[29] W.W. Moses and S.E. Derenzo, IEEE Trans. Nucl. Sci. NS-36 (1989) 173.

[30] S.E. Derenzo, W.W. Moses, J.L. Cahoon, T.A. Devol and L.A. Boatner, in Conference Record of the 1991 IEEE Nuclear Science Symp. and Medical Imaging Conference, Vol. 1, ed. F. Kirsten (IEEE, Piscataway, 1991), p. 143.

[31] C. Pédrini, B. Moine, J.C. Gacon and B. Jacquier, J. Phys.: Condens. Matter 4 (1992) 5461.

[32] C. Pédrini, B. Moine, D. Bouttet, A.N. Belsky, V.V. Mikhailin, A.N. Vasil'ev and E.I. Zinin, Chem. Phys. Lett. 206 (1993) 470.

[33] M. Nikl, J.A. Mares, E. Mihokova, A. Beitlerova, K. Blazek and J. Jindra, Solid State. Commun. 87 (1993) 185.

[34] R.T. Williams, E.D. Thoma and P.H. Bunton, Mat. Res. Soc. Symp. Proc. 348 (1994) 331.

[35] E. Auffray, T. Beckers, R. Chipaux, I. Dafinei, P. Depasse, H. El Mamouni, J.L. Faure, J. Fay, H. Hillemanns, B. Ille, P. Lebrun, P. Lecoq, J. Nelissen, M. Nikl, R. Raghavan, A. Rosowsky, D. Schmitz and M. Schneegans, Mat. Res. Soc. Symp. Proc. 348 (1994) 117.

[36] W.W. Moses, private communication 10/94.

[37] Y. Toyozawa, Rev. Solid State Sci. 4 (1990) 3; Proc. US–Japan Seminar on Atomic Processes Induced by Electronioc Excitation in Non-Metallic Solids, September 11–15, 1989.

[38] Y. Unuma, Y. Masumoto, S. Shionoya and H. Nishimura, J. Phys. Soc. Japan 52 (1983) 4277.

[39] E. Laredo, L.G. Rowan and L. Slifkin, Phys. Rev. Lett. 47 (1981) 384.

[40] Z. A. Rachko and J. A. Valbis, Phys. Stat. Sol. b 93 (1979) 161.

[41] A.L. Shluger, R.W. Grimes, C.R.A. Catlow and N. Itoh, J. Phys.: Condens. Matter 3 (1991) 8027.

[42] D.J. Chadi and K.J. Chang, Phys. Rev. B 39 (1989) 10063.

[43] J.E. Dmochoski, J.M. Langer, Z. Kalinski and W. Jantsch, Phys. Rev. Lett. 56 (1986) 1735; Yang Cai and K.S. Song, J. Phys.: Condens. Matter 7 (1995) 2275.

[44] Y. Shinozuka and Y. Toyozawa, J. Phys. Soc. Japan. 46 (1979) 505.; Y. Toyozawa, Physica B 116 (1983)7.